RSC Advances

PAPER

View Article Online
View Journal | View Issue

Cite this: *RSC Adv.*, 2015, **5**, 17438

Ultrafast chemical lithiation of single crystalline silicon nanowires: *in situ* characterization and first principles modeling†

Jong-Hyun Seo,‡[ab] Chia-Yun Chou,‡[c] Yu-Hao Tsai,[c] Yigil Cho,[d] Tae-Yeon Seong,[b] Woo-Jung Lee,[e] Mann-Ho Cho,[e] Jae-Pyoung Ahn,[a] Gyeong S. Hwang*[cf] and In-Suk Choi*[d]

Received 20th November 2014
Accepted 30th January 2015

DOI: 10.1039/c4ra14953j

www.rsc.org/advances

Through a combined density functional theory and *in situ* scanning electron microscopy study, we provide evidence of the ultrafast chemical lithiation of a single crystalline Si nanowire which is brought into direct contact with Li metal in the absence of an applied external electric field. Unlike the previous *in situ* lithiation results, the ultra-fast lithiation process in this study is purely driven by the concentration gradient and is found to be limited by Li diffusion through the pristine/lithiated Si phase boundary. The experimental and calculated lithiation speeds are in excellent agreement at around 1 μm s^{-1}, corresponding to a high Li diffusivity value of about 10^{-9} cm^2 s^{-1}. The improved understanding of lithiation kinetics may contribute to the design of higher-power Si-based anodes.

Introduction

Silicon (Si) has recently emerged as an attractive anode material for lithium-ion batteries (LIBs) because of its impressive energy storage capacity. Among all the potential anode materials, Si has the highest known theoretical capacity,[1–4] which is one order of magnitude larger than that of graphite (the most commonly used anode in today's Li-ion batteries).[4–6] However, alloying Li with Si is a different process from Li insertion in graphite (*via* intercalation mechanism). The alloying-induced structural and volume changes (>300%) can cause pulverization, loss of electrical contact and consequently early capacity fading.[2–4,7–9] In order to overcome this drawback, many studies have approached the cyclability issue *via* structural modifications in the nanosize range.[1,10–14] It has been shown that because of the high surface-to-volume ratio, nanostructured Si can better accommodate strain and limit crack propagation, while the shorter diffusion distances for Li atoms offer the additional advantage of faster charging/discharging rates.[1,15–17] In recent years, a number of published works on Si have realized stable charge–discharge capacities over 1200 mA h g^{-1} for more than 1000 cycles,[18] suggesting a great potential for application in LIBs.

Benefited by the development of *in situ* test methods in electron microscopy (EM) and rapid advancement of atomistic scale modeling, significant progress has been made in the understanding of lithiation-induced structural evolution in nanostructured Si-based anodes.[19–21] However, an affirmative description of Li kinetics in Si nanostructures is still very limited, and the experimentally measured Li diffusivity (D_{Li}) values are measured *via* electrochemical testing which vary by six orders of magnitude depending on the sample and test conditions.[19,22–24] Furthermore, since the conventional electrochemical approaches to D_{Li} determination are based on an averaged property from *ex situ* measurements, it is very difficult to characterize Li diffusion inside an individual nanowire and differentiate which from diffusion in electrolyte, through the complex solid-electrode-interface (SEI), and inside lithiated Si with varying Li concentrations.

In this paper, we present a combined experimental and theoretical investigation on the chemical lithiation of individual Si nanowires (NWs), which are brought to direct contact with Li metal inside a scanning microscope (SEM) in the absence of an applied electric field. Upon lithiation, the structural evolution is monitored *in situ*, allowing us to estimate the propagation speed of the lithiation front which is faster than

[a]*Advanced Analysis Center, Korea Institute of Science and Technology, Seoul 130-650, South Korea*

[b]*Department of Materials Science and Engineering, Korea University, Seoul 136-701, South Korea*

[c]*Materials Science and Engineering Program, University of Texas at Austin, Austin, Texas 78712, USA. E-mail: gshwang@che.utexas.edu; Fax: +1 512 471 0542; Tel: +1 512 471 4847*

[d]*High Temperature Energy Materials Research Center, Korea Institute of Science and Technology, Seoul 130-650, South Korea. E-mail: insukchoi@kist.re.kr; Fax: +82 2 958 5449; Tel: +82 2 958 6622*

[e]*Institute of Physics and Applied Physics, Yonsei University, Seoul 120-749, Korea*

[f]*Department of Chemical Engineering, University of Texas at Austin, Austin, TX 78712, USA*

† Electronic supplementary information (ESI) available. See DOI: 10.1039/c4ra14953j

‡ These authors are contributed equally to this work.

that of the previously reported ultra-fast lithiation of SiNWs,[22] and correlate which with D_{Li} across the phase boundary between the lithiated and pristine Si. Together with the DFT investigations, we are able to explain the lithiation mechanism and more importantly reveal the genuine features of Li transport in lithiated SiNWs for the first time.

Experimental

Fabrication of single crystalline Si nanowires

Si NWs with [111] axial orientation were synthesized on the Si (111) substrate with Au catalyst by the vapor–liquid–solid (VLS) method using an ultrahigh vacuum chemical vapor deposition (CVD) system. A 2 nm thick Au film (as a catalyst) was deposited on a cleaned Si (111) substrate in a metal growth chamber at a growth pressure of $\sim 5 \times 10^{-7}$ Torr by thermal evaporation. After the formation of Au droplets through annealing, Si NWs were synthesized by filling the main chamber with a mixture of SiH_4 as precursors, and H_2 as the carrier gas, while maintaining a fixed total pressure of 2 Torr. The process temperature was set to 400–450 °C at Au–Si eutectic temperatures. The dimension of grown Si NWs is approximately 2–3 μm in length and 70–110 nm in diameter as shown in Fig. S1.† The more detailed information of synthesis and the structure of NWs are provided in the ESI.†

In situ direct contact lithiation

The direct solid state lithiation test without an external electrical potential was performed using a nanomanipulator (MM3A, Kleindiek). To avoid oxidation, the entire process was carried out inside the dual beam focused ion beam chamber (FIB, Quanta 3D, FEI). We transferred a Si nanowire from the substrate to the nanomanipulator tungsten tip by Pt deposition in the FIB chamber. The bulk Li was cut inside the chamber to make a pristine surface. Subsequently, we translated the harvested Si NW to the bulk Li and made direct contact of the fractured side end of the Si NW to the surface of the bulk Li. Please see Fig. S2 for the schematic of the method in the ESI.† The whole process of the lithiation was exposed to the electron beam in SEM. Therefore it may be possible to accumulate charges at different materials. However the tungsten probe and stage are grounded so electron beam dose not have an effect on lithiation behavior. Moreover we confirmed that the lithiation behavior indeed occurs when the electron beam is turned off.

Computational methods

Quantum mechanical calculations reported herein were performed on the basis of density functional theory (DFT) within the generalized gradient approximation (GGA-PW91), as implemented in the Vienna *Ab initio* Simulation Package (VASP). The projected augmented wave (PAW) method with a plane-wave basis set was used to describe the interaction between core and valence electrons. An energy cutoff of 350 eV was used for geometric optimization of model structures for (i) *a*-LiSi and *a*-Li_2Si, and (ii) *a*-Li_4Si/Si(110) interface; all atoms were fully relaxed using the conjugate gradient method till residual forces are smaller than 5×10^{-2} eV $Å^{-1}$. For Brillouin zone sampling, sufficient *k*-point mesh was used in the scheme of Monkorst–Pack. To simulate the diffusion and chemical lithiation processes, *ab initio* molecular dynamics (AIMD) simulations were performed at the temperatures of interest; a time step of 1 fs was used while the temperature was controlled *via* Nose–Hover thermostat. For more detailed simulation methods, please refer to the ESI.†

Results and discussions

In situ characterization of chemical lithiation

Fig. 1 shows the microstructural evolution of a pristine Si [111] nanowire (SiNW), which was brought into direct contact with Li metal at room temperature in vacuum, without an external electric field (see ESI, Fig. S1, S2 and Movie 1† for detailed experimental methods and real-time *in situ* lithiation behavior). At $t = 0.00$ s, the pristine SiNW was straight with a uniform diameter around 78.9 nm. Once the nanowire contacted bulk Li, it exhibited significant morphological changes captured in the time-lapse series of SEM images up to $t = 1.02$ s. Li atoms near the vicinity of the Li–Si contacting area diffused into the Si nanowire, and volume expansion occurred instantaneously as the effective reaction front (marked by the yellow triangle) propagated rapidly from the nanowire tip towards the other end. At $t = 1.02$, the entire SiNW swelled uniformly in the radial direction without noticeable elongation or bending.

The cross-section becomes circular after lithiation and the total volume expansion is estimated around 330% which is comparable to that of a highly lithiated Si alloy (see ESI, Fig. S3 and S5†).[16] The scanning transmission electron microscope (STEM) and electron energy loss spectroscopy (EELS) analyses later confirmed the complete amorphization in the center of the lithiated SiNW (see ESI, Fig. S4†). Different from the conventional electrochemical lithiation, our results clearly demonstrate that lithiation of a SiNW can occur in the absence of an external electric field; this is also well supported by our simulations investigating the onset of lithiation at Si surfaces and Li/Si interfaces (see ESI, Fig. S6†) as well as the previous work by Johari *et al.*[25] More fundamental explanation regarding the lithiation mechanism and kinetics will be discussed along with the results from our atomistic simulations.

By precisely tracking the reaction front movement (Fig. 1 and Movie 1†), we estimated the lithiation propagation speed to be around 1082 nm s^{-1}, which is at least two orders of magnitude higher than what was reported for electrochemically lithiated SiNWs, and even five times faster than the so-called ultra-fast lithiation speed (the record-high lithiation speed of carbon coating enhanced SiNWs).[22] Furthermore, our *in situ* SEM study also provides insight into the kinetics of SiNW lithiation without the influences from the applied electrical field and complex reactions at the solid-electrolyte-interface (SEI). In conventional electrochemical lithiation tests, four kinetic processes are commonly considered to have effects on the rate of lithiation: (i) Li ion diffusion in the electrolyte, (ii) the redox reaction at the electrolyte/Si interface, (iii) the formation of lithiated Si (*a*-Li_xSi) at the interface between *a*-Li_xSi and *c*-Si, and (iv) diffusion of the neutralized Li atoms in *a*-Li_xSi. Upon

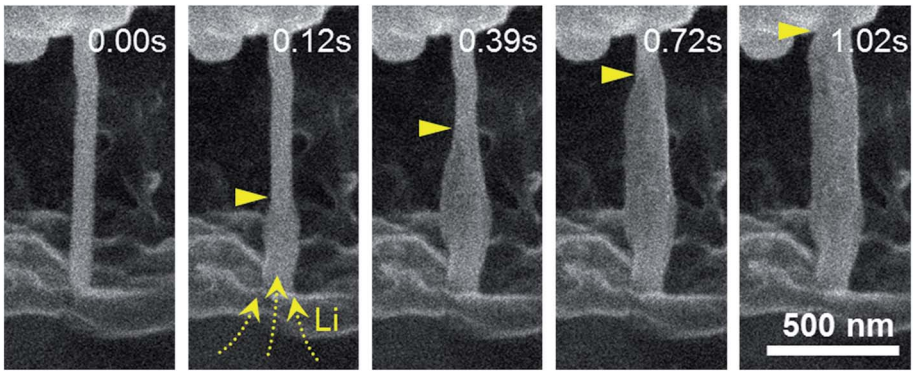

Fig. 1 Ultrafast chemical lithiation of a Si NW. Microstructural evolution of an intrinsic Si [111] nanowire in direct contact with Li metal was monitored. Volume expansion occurred instantaneously as the effective reaction front (marked by the yellow triangle) propagated from the nanowire tip towards the other end.

lithiation, Li cations (Li^+) at the electrolyte/Si interface must combine with electrons (redox reaction) before the neutralized Li atoms can start diffusing into the Si anode. However, *via* the lithiation technique employed in this study, we are able to rule out the first two factors while providing a perfect controlled environment to examine the later two factors as follows.

If the *a*-Li_xSi alloy formation were the dominant rate-limiting factor for the lithiation speed, the corresponding length of the reaction front propagation (h) would be linearly proportional to the time (t). Otherwise, if the propagation of the effective reaction front were controlled by Li atom diffusion, the relation between h and t would followed the one-dimensional Random Walk diffusion model; $h^2 = nDt$, where n is a numerical constant depending on dimensionality and D is the diffusivity (in the reaction front advancing direction). According to the experimental results shown in Fig. 2, h^2 is linearly proportional to t (that is $h^2\ t^{-1} = 1.03$), which confirms Li diffusion to be the dominant rate-limiting factor. Given one-dimensional diffusion, the Li diffusivity (D_{Li}) can be estimated around 2.58×10^{-9} $cm^2\ s^{-1}$ based on $D = h^2/(4\ t)$.

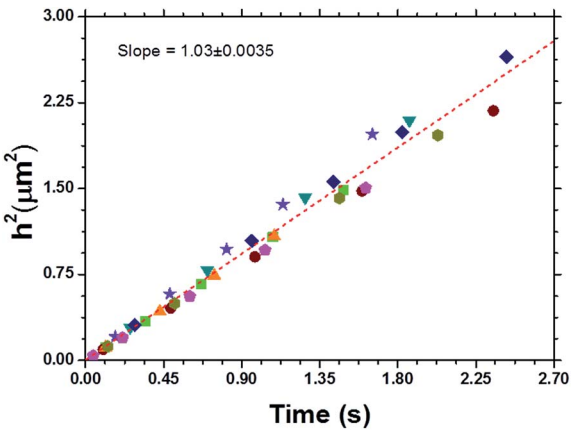

Fig. 2 The experimental plot of the length of the effective reaction front propagation (h) *vs.* the lithiation time (t). h^2 is linearly proportional to t ($h^2\ t^{-1} = 1.03$), which strongly suggests Li diffusion to be the dominant rate-limiting factor. Plots were from the nine measurements.

Computation modelling of chemical lithiation

Still, the theoretical understanding of this diffusion-controlled chemical lithiation is very limited. Fig. 3a shows a schematic illustration of the potential- and electrolyte-free lithiation process considered in the present work based on the following rationales. Firstly, for a SiNW, the lithiation process is found to proceed faster along the outer surfaces than near the center.[17,26–28] Secondly, according to previous experimental and theoretical studies,[21,29] the lithiation process is much faster in the ⟨110⟩ direction, as compared to the ⟨111⟩ direction. Therefore, we can expect the lithiation of [111] SiNWs to initiate preferentially at the {110} facets. Moreover, with increasing Li contents, D_{Li} in Si tends to increase by orders of magnitude (Fig. 3b);[28,30,31] this suggests that room-temperature lithiation is kinetically feasible that converts the outer surface of the *c*-SiNW into *a*-Li_xSi with x close to 4 as is in line with previously theoretical and experimental results.[32,33]

Given the facile Li diffusion in a highly lithiated *a*-Li_xSi phase, the migration of the *a*-Li_xSi/Si(110) phase boundary near the effective reaction front, which is described in the enlarged figure in Fig. 3a, may likely be a main rate-limiting step of the entire lithiation speed. To capture the structural evolution concurrent with Li diffusion at the given phase boundary, a model cell consisting of *a*-Li_xSi (with x close to 4) interfaced with Si (110) facet was constructed and annealed *via ab initio* molecular dynamics (AIMD) simulations at 1000 K. Starting with the initial configuration ($t = 0$ ps), the supercell after different MD time steps ($t = 4$, 8 and 16 ps) representing different stages of lithiation are shown in Fig. 4. Driven by the concentration gradient, Li atoms from the *a*-Li_4Si phase are diffusing across the sharp amorphous–crystalline-interface (ACI) into the *c*-Si matrix. The weakened *c*-Si lattice (Si_A–Si_B and Si_C–Si_B bonds) eventually breaks off as dumbbells (Si_D–Si_B) and dissolves into the *a*-Li_4Si phase while the lithiation front advances into the pristine *c*-Si region. In a 'layer-by-layer' fashion, the lithiation process proceeds as the lithiation front advances approximately 4 Å in 16 ps.

Due to the difference in temperature, we cannot directly compare the calculated lithiation propagation speed (around 0.25 Å ps^{-1} at 1000 K) to the experimentally observed value

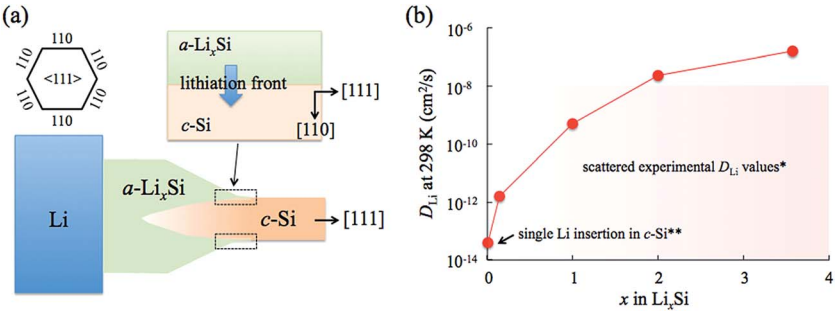

Fig. 3 (a) Schematic illustration of the chemical lithiation model of a [111] SiNW. The enlarged figure for the black dotted box illustrates *a*-Li$_x$Si/Si(110) phase boundary near the effective reaction front. The phase boundary (the lithiation front) moves from the outers surface into the center, which is rationalized as the rate limiting step of the propagation of the effective reaction front. (b) Variations in diffusivity (D_{Li}) of Li atoms in *a*-Li$_x$Si alloys of selected Li contents ($x = 0.02$, 0.14, 1, 2 and 3.57) at 298 K; an example of how D_{Li} can be predicted based on AIMD simulations is shown in Fig. S7. For comparison, the scattered experimental D_{Li} values and D_{Li} calculated for a single Li in *c*-Si are indicated by *[28] and **,[30] respectively.

(around 1 μm s^{-1} at 298 K). However, based on the one-dimensional Random Walk diffusion model ($l^2 = 2Dt$, where l is the length of the lithiation front propagation, D is the diffusivity and t is time), we could relate the lithiation propagation speed to a D_{Li} value (*i.e.*, the simulated lithiation propagation speed of 0.25 Å ps^{-1} renders a D_{Li} value on the order of 10^{-5} cm^2 s^{-1} and $E_a \approx 0.3$ eV at 1000 K). Next, considering the temperature-dependent Arrhenius diffusion equation $D = D_0 \exp(-E_a/kT)$ and assuming the prefactor $D_0 \approx 10^{-3}$ cm^2 s^{-1},[28,30,34] we could approximate the D_{Li} value to be on the order of 10^{-9} cm^2 s^{-1} at room temperature (298 K), which is in excellent agreement with the value estimated based on the *in situ h* measurement; $D_{Li} = h^2/(4\,t) = 2.58 \times 10^{-9}$ cm^2 s^{-1}. In comparison to the wide range of experimentally measured D_{Li} values in the literature (from 10^{-14} to 10^{-8} cm^2 s^{-1}), our value is within the range but on the higher side, which coincides with the unprecedentedly fast lithiation process. The excellent fit between theoretical and experimental results clearly demonstrated that (i) driven by the concentration difference, lithiation of a SiNW can rapidly occur in the absence of an external electric field; (ii) the lithiation rate of a [111] SiNW may predominantly be controlled by the propagation of the *a*-Li$_x$Si/Si(110) interface as Li atoms continuously diffuse into the *c*-Si matrix leading to the advancing reaction front.

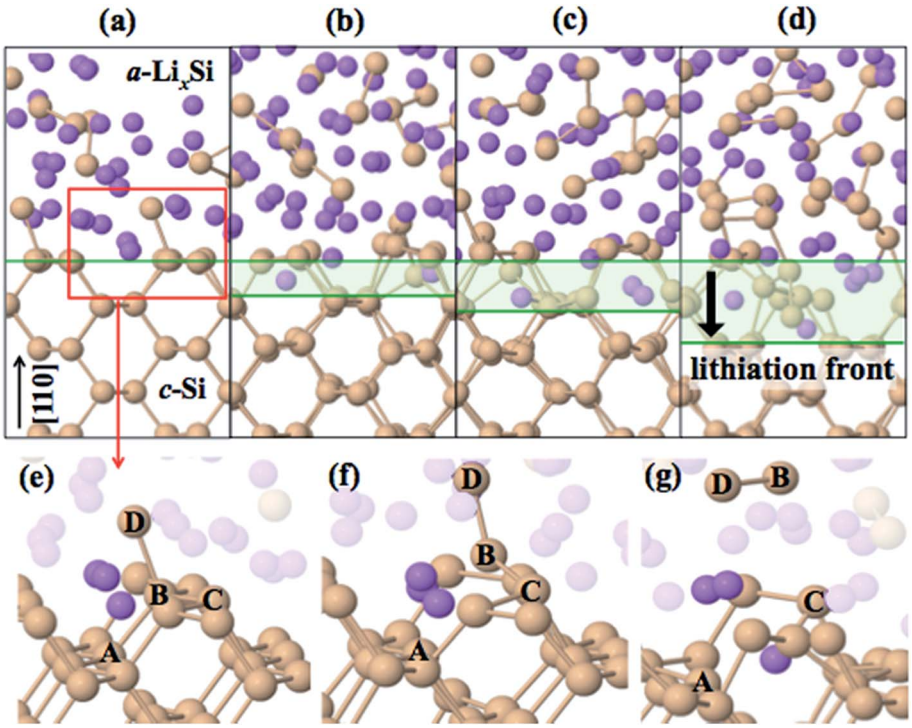

Fig. 4 AIMD simulation to capture the structure evolution of the *a*-Li$_x$Si/Si(110) phase boundary at various stages of lithiation; structures shown in (a) to (d) correspond to the starting $t = 0$ and after 4, 8 and 16 ps of annealing at 1000 K. The break off of Si–Si dumbbells is captured in configurations shown in (e) to (g).

Conclusions

In conclusion, we employed a combined effort of *in situ* SEM experiments and DFT calculations to investigate the concentration-gradient-driven lithiation process in individual Si nanowires (SiNWs). Through this new potential- and electrolyte-free lithiation method, we were able to examine the genuine features of Li transport in a lithiated SiNW for the first time. The key findings of this can be summarized as follows: first, upon direct contact with Li metal, the concentration gradient is sufficient to drive the lithiation of SiNW without an applied external electrical field, which is well explained by our theoretical prediction. Similar to the electrochemically lithiated SiNWs, the chemically lithiated SiNW was also found to swell uniformly in the radial direction without noticeable elongation or bending; the total volume expansion is estimated around 330%. Second, *in situ* SEM characterization allowed us to precisely track the reaction front movement, providing significant insight into the lithiation kinetics of single crystalline SiNW. The speed of lithiation front is 1082 nm s^{-1} corresponding to the fastest lithiation speed ever recorded. We found that the square of the propagation length (h^2) is linearly proportional to the lithiation time (t), suggesting the speed of Si lithiation is controlled by how fast Li atoms diffuse across the phase boundary into the pristine *c*-Si; the Li diffusivity is estimated around $D_{Li} = 2.58 \times 10^{-9}$ cm^2 s^{-1}. Finally, the observed lithiation mechanism is then cross-examined by DFT investigation, where the rate-limiting step is modeled by the propagation of the *a*-Li_xSi/Si(110) phase boundary. The predicted room-temperature D_{Li} ($\approx 10^{-9}$ cm^2 s^{-1}) from our AIMD simulations is in excellent agreement with the experimentally estimated value. Our study clearly highlights that ultrafast SiNW lithiation can be solely driven by the concentration gradient in the absence of external electric field, which implies that the fast lithiation speed is primarily controlled by Li diffusion across the lithiated and pristine Si phase boundary. The fundamental findings from the combined experimental and theoretical study may extend the understanding of the lithiation kinetics in SiNWs and thereby improve the design of Si-based anodes for advanced high power LIBs.

Acknowledgements

This work was supported by KIST R&D program of 2Z04520, NST program (Grant number: Yunghap-13-1-KIST) (ISC) and the Robert A. Welch Foundation (Grant number: F-1535) (GSH). We would also like to thank the Texas Advanced Computing Center for use of their computing resources.

References

1 C. K. Chan, H. Peng, G. Liu, K. Mcilwrath, X. F. Zhang, R. A. Huggins and Y. Cui, *Nat. Nanotechnol.*, 2007, **3**, 31–35.
2 B. A. Boukamp, G. C. Lesh and R. A. Huggins, *J. Electrochem. Soc.*, 1981, **128**, 725–729.
3 M. N. Obrovac and L. Christensen, *Electrochem. Solid-State Lett.*, 2004, **5**, A93–A96.
4 T. D. Hatchard and J. R. Dahn, *J. Electrochem. Soc.*, 2004, **151**, A838–A842.
5 L. Baggetto, R. A. H. Niessen, F. Roozeboom and P. H. L. Notten, *Adv. Funct. Mater.*, 2008, **18**, 1057–1066.
6 M. Green, E. Fielder, B. Scrosati, M. Wachtler and J. S. Moreno, *Electrochem. Solid-State Lett.*, 2003, **6**, A75–A79.
7 J. Yang, M. Winter and J. O. Besenhard, *Solid State Ionics*, 1996, **90**, 281–287.
8 U. Kasavajjula, C. Wang and A. J. Appleby, *J. Power Sources*, 2007, **163**, 1003–1039.
9 J. P. Maranchi, A. F. Hepp, A. G. Evans, N. T. Nuhfer and P. N. Kumta, *J. Electrochem. Soc.*, 2006, **153**, A1246–A1253.
10 T. Takamura, S. Ohara, M. Uehara, J. Suzuki and K. Sekine, *J. Power Sources*, 2004, **129**, 96–100.
11 X. Xiao, P. Liu, M. W. Verbrugge, H. Haftbaradaran and H. Gao, *J. Power Sources*, 2011, **196**, 1409–1416.
12 I. Ryu, J. W. Choi, Y. Cui and W. D. Nix, *J. Mech. Phys. Solids*, 2011, **59**, 1717–1730.
13 X. H. Liu, L. Zhong, S. Huang, S. X. Mao, T. Zhu and J. Y. Huang, *ACS Nano*, 2012, **6**, 1522–1531.
14 B. Gao, S. Sinha, L. Fleming and O. Zhou, *Adv. Mater.*, 2001, **31**, 816–819.
15 J. L. Goldman, B. R. Long, A. A. Gewirth and R. G. Nuzzo, *Adv. Funct. Mater.*, 2011, **21**, 2412–2422.
16 S. W. Lee, M. T. McDowell, J. W. Choi and Y. Cui, *Nano Lett.*, 2011, **11**, 3034–3039.
17 Q. Zhang, W. Zhang, W. Wan, Y. Cui and E. Wang, *Nano Lett.*, 2010, **10**, 3243–3249.
18 H. Wu, G. Yu, L. Pan, N. Liu, M. T. McDowell, Z. Bao and Y. Cui, *Nat. Commun.*, 2012, **4**, 1943–1948.
19 X. H. Liu, J. W. Wang, S. Huang, F. Fan, X. Huang, Y. Liu, S. Krylyuk, J. Yoo, S. A. Dayeh, A. V. Davydov, S. X. Mao, S. T. Picraux, S. Zhang, J. Li, T. Zhu and J. Y. Huang, *Nat. Nanotechnol.*, 2012, **7**, 749–756.
20 M. T. McDowell, S. W. Lee, C. Wang and Y. Cui, *Nano Energy*, 2012, **1**, 401–410.
21 X. H. Liu, Y. Liu, A. Kushima, S. Zhang, T. Zhu, J. Li and J. Y. Huang, *Adv. Energy Mater.*, 2012, **2**, 722–741.
22 X. H. Liu, L. Q. Zhang, L. Zhong, Y. Liu, J. W. Wang, J.-H. Cho, S. A. Dayeh, S. T. Picraux, J. P. Sullivan, S. X. Mao, Z. Z. Ye and J. Y. Huang, *Nano Lett.*, 2011, **11**, 2251–2258.
23 N. Balke, S. Jesse, Y. Kim, L. Adamczyk, A. Tselev, I. N. Ivanov, N. J. Dudney and S. V. Kalinin, *Nano Lett.*, 2010, **10**, 3420–3425.
24 E. M. Pell, *Phys. Rev.*, 1960, **119**, 1014–1021.
25 P. Johari, Y. Qi and V. B. Shenoy, *Nano Lett.*, 2011, **11**, 5494–5500.
26 T.-L. Chan and J. R. Chelikowsky, *Nano Lett.*, 2010, **10**, 821–825.
27 X. H. Liu, H. Zheng, L. Zhong, S. Huang, K. Karki, L. Q. Zhang, Y. Liu, A. Kushima, W. T. Liang, J. W. Wang, J. H. Cho, E. Epstein, S. A. Dayeh, S. T. Picraux, T. Zhu, J. Li, J. P. Jullivan, J. Cumings, C. Wang, S. X. Mao, Z. Z. Ye, S. Zhang and J. Y. Huang, *Nano Lett.*, 2011, **11**, 3312–3318.
28 C.-Y. Chou and G. S. Hwang, *Surf. Sci.*, 2013, **612**, 16–23.

29 M. K. Y. Chan, C. Wolverton and J. P. Greeley, *J. Am. Chem. Soc.*, 2012, **134**, 14362–14374.
30 H. Kim, K. E. Kweon, C.-Y. Chou, J. G. Ekerdt and G. S. Hwang, *J. Phys. Chem. C*, 2010, **114**, 17942–17946.
31 Z. Cui, F. Gao, Z. Cui and J. Qu, *J. Power Sources*, 2012, **207**, 150–159.
32 H. Kim, C.-Y. Chou, J. G. Ekerdt and G. S. Hwang, *J. Phys. Chem. C*, 2011, **115**, 2514–2521.
33 P. Limthongkul, Y.-I. Jang, N. J. Dudney and Y.-M. Chiang, *Acta Mater.*, 2003, **51**, 1103–1113.
34 X. R. Wang, X. Xiao and Z. Zhang, *Surf. Sci.*, 2002, **512**, 361–366.